RESEARCH ARTICLE
PLANETARY SCIENCES

Earth and Planetary Physics
8: 899–909, 2024
doi: 10.26464/epp2024061

Parameter optimization for Rayleigh–Mie lidar under different dust conditions for the landing area of Martian Tianwen-1

KeXin Ming[1], Chong Wang[1,2*], XiangHui Xue[1,2,3], JianFei Wu[1,3], and TingDi Chen[1,3]

[1]School of Earth and Space Sciences, University of Science and Technology of China, Hefei 230026, China;

[2]Anhui Mengcheng Geophysics National Observation and Research Station, University of Science and Technology of China, Hefei 230026, China;

[3]Hefei National Laboratory, Hefei 230088, China

Key Points:

- The lidar was mathematically modeled, and the correctness of the model was verified by using real lidar measurement data.
- The landing area of Tianwen-1 was selected, the Martian atmospheric mode was incorporated into the lidar model, and the backscatter signals and key parameters of the Mie–Rayleigh lidar under the conditions of a clean Martian atmosphere and a global sandstorm were systematically analyzed.
- The optimal detection altitude range of Mie scattering and Rayleigh scattering on Mars under different atmospheric conditions was obtained.

Citation: Ming, K. X., Wang, C., Xue, X. H., Wu, J. F., and Chen, T. D. (2024). Parameter optimization for Rayleigh–Mie lidar under different dust conditions for the landing area of Martian Tianwen-1. *Earth Planet. Phys.*, *8*(6), 899–909. http://doi.org/10.26464/epp2024061

Abstract: Mars is the terrestrial planet in the solar system that is closest to the Earth. Studying the atmospheric parameters of Mars and studying the evolutionary history of the Martian environment on this basis is helpful for people to discover signs of extraterrestrial life and to study the trend of climate change on Earth. Mie–Rayleigh scattering lidar is an important technology for detecting parameters from the surface to the middle and upper atmosphere. Because of the different aerosol distributions, Mie scattering and Rayleigh scattering have their own optimal detection ranges. Given the long period and high cost of any deep space exploration program, it is important to conduct sufficient feasibility studies and parameter simulations before the payload is launched. In this study, a parameterized lidar mathematical model and Earth's atmospheric mode are used to compare with the measured signals of ground-based Mie–Rayleigh scattering lidar, and the correctness of the lidar mathematical model is verified. Using the model, we select the landing area of Tianwen-1 and substitute it into the Martian atmospheric mode, and then the Mie–Rayleigh lidar backscattering signal and the key parameters of the lidar system are systematically analyzed under the conditions of a clean Martian atmosphere and a global sandstorm. In addition, the optimal detection altitude ranges of Mie scattering and Rayleigh scattering on Mars under different atmospheric conditions are obtained, which provides a reference for the practical design and development of the subsequent lidar system for the Martian atmospheric environment.

Keywords: lidar; Martian atmospheric mode; Mie scattering; Rayleigh scattering

1. Introduction

Deep space exploration is currently a very important development direction that has attracted the attention of countries worldwide. The atmospheric exploration of terrestrial planets is a particularly important and indispensable part of deep space exploration. Mars, as a planet in the solar system whose environment is closest to the Earth, is also a typical representative of terrestrial planets. Many climatologists have suggested that studying the current Martian environment and extrapolating the evolutionary history of the Martian environment on that basis will greatly help people understand the direction and trend of climate change on Earth. Another significant reason for humans to focus on Mars is that current research shows that Mars is one of the easiest and most likely planets to colonize. Detection of the parametric characteristics of the Martian atmosphere is one of the most important tasks in Mars exploration. As a vital means of active detection of atmospheric parameters, a lidar system has the advantages of multiple detection parameters and a high spatiotemporal resolution, and it has been verified to have ground, airborne, and spaceborne capabilities on Earth (Frehlich et al., 1994; Asaka et al., 2001; Li ZG et al., 2016; Sun XL et al., 2017; Li YD et al., 2022; Yakovlev et al., 2022). In 2013, the University of Science and Technology of China developed a Rayleigh scattering lidar system that emits a laser wavelength of 355 nm and can realize the detection of atmospheric wind fields within a vertical distance of 15–60 km altitude (Dou XK et al., 2014). On August 22, 2018, the European Space Agency launched the Atmospheric Dynamics Mission Aeolus, which had been in development for decades. The satellite is equipped with a dual-

First author: K. X. Ming, mingkx@mail.ustc.edu.cn
Correspondence to: C. Wang, wclhy50@ustc.edu.cn
Received 19 MAR 2024; Accepted 30 JUL 2024.
First Published online 24 SEP 2024.

wavelength incoherent wind lidar system called ALADIN (Atmospheric LAser Doppler INstrument; Paffrath et al., 2009; Reitebuch et al., 2009), which can simultaneously measure Rayleigh scattering signals and Mie scattering signals and can detect atmospheric wind field profiles within a vertical distance of 0–30 km altitude. In 2021, Shen FH et al. (2021) proposed a Rayleigh Doppler lidar based on quad Fabry–Perot standard instruments, which can accurately detect wind speed, temperature, and aerosols at altitudes from 0.2 to 60 km. The structure of the lidar system was described in detail, and its performance was simulated. Compared with traditional lidar systems, lidar systems for deep space detection are more expensive and have higher requirements for system stability. Therefore, to ensure the effectiveness of the lidar system in the application of Mars atmospheric exploration, it is necessary to conduct sufficient research and parameter design in the early stages.

Human curiosity about Mars was first evident in the late 16th century, but the real attempt to explore Mars began in the 1960s. To date, among the various attempts around the world to explore Mars, only the Phoenix lander launched by the United States was equipped with an aerosol MSCATTER (Mie SCATTER) lidar system (Whiteway et al., 2008). This lander was the first and, thus far, has been the only one on which a lidar system has completed atmospheric exploration missions on Mars (Komguem et al., 2013). With the rapid development of lidar technology, more and more researchers have realized that a lidar system is a very powerful payload technology in deep space exploration. In 2015, the National Aeronautics and Space Administration (NASA) and the University of Hawaii jointly developed a multisensor system test prototype for detection of the material composition on the surface of Europa and Mars, which included an aerosol lidar system (Abedin et al., 2015). This lidar system could distinguish the composition of the atmosphere within a distance of 100 m during experimental measurements. In 2018, Cremons et al., (2018) designed and tested a prototype wind lidar for direct detection of the atmosphere in orbit around Mars at the Goddard Geophysical Observatory. The test results showed that the atmospheric backscattering coefficient profile and wind field profile measured by the prototype were highly consistent with the Environmental Modeling Center meteorological model, which demonstrates the rationality and feasibility of the system. At the same time, the team of Hong GL (2018) from the Shanghai Institute of Technical Physics of the Chinese Academy of Sciences conducted a theoretical analysis of the detection performance and feasibility of the lidar system when working on the surface of Mars.

In this paper, the performance of Mie–Rayleigh scattering lidar in different environments is studied and discussed, and an innovative Mars atmospheric model is introduced, which provides a reference for the development of an atmospheric detection lidar system for payloads. In the second section, the mathematical model and atmospheric model of the Mie–Rayleigh scattering lidar system are described. In the third section, the specific parameters of the Mie–Rayleigh scattering lidar system used in the simulation are introduced, and the backscattering signal and signal-to-noise ratio results obtained by the simulation are explained. In the fourth section, the simulation results of the lidar system in the Martian atmospheric model are analyzed in detail. The fifth section gives concise conclusions.

2. Model of the Mie–Rayleigh Scattering Lidar System

2.1 Lidar Equation

In the process of atmospheric propagation, the laser emitted by the lidar system will have a scattering effect with various material components in the atmosphere, and the scattered light will be emitted in all directions. The lidar system usually receives the backscattering light signal only to reverse the characteristics of the scatterer. When only single scattering is considered, the lidar equation can be expressed as follows (Fernald, 1984):

$$N(\lambda, z) = N_0(\lambda_0)[\beta(\lambda, \lambda_0, z, \theta)\Delta z \cdot \left[\frac{A}{z^2}\right] O(z)\eta(\lambda, \lambda_0) \mathrm{e}^{\int_0^z -\alpha(\lambda_0,\xi)\mathrm{d}\xi} \mathrm{e}^{\int_0^z -\alpha(\lambda,\xi)\mathrm{d}\xi} + N_B, \tag{1}$$

where $N(\lambda, z)$ is the power of the backscattering signal received by the lidar in the altitude interval ($z - \Delta z/2$， $z + \Delta z/2$), $N_0(\lambda_0)$ represents the laser emission power, $\beta(\lambda, \lambda_0, z, \theta)$ is the backscattering coefficient, Δz denotes the height resolution, and A is the telescope receiving area. Obviously, the larger the receiving area of the telescope is, the stronger the received backscattering signal will be. Variable $O(z)$ is the overlap factor; in general, the laser beam will not enter the telescope field of view until after a certain distance, and thereafter, the overlap factor will always be 1. In addition, $\eta(\lambda)$ denotes the efficiency of the lidar system; $\alpha(\lambda_0, z)$ is the extinction coefficient of the laser light emitted by the lidar system on the incident path; $\mathrm{e}^{-\int \alpha(\lambda_0,\xi)\mathrm{d}\xi}$ represents the transmittance of the laser light on the one-way path from emission to the scatterer; and $\alpha(\lambda, z)$ is the extinction coefficient of the scattered light after the interaction of the laser light with the scatterer. The expression $\mathrm{e}^{-\int \alpha(\lambda,\xi)\mathrm{d}\xi}$ represents the transmittance of the scattered light on the one-way path of the laser and the scattered light to be received by the telescope, whereas N_B indicates the background light in the sky.

The lidar equation has two unknown parameters, the backscattering coefficient and the extinction coefficient, which theoretically cannot be solved directly. We adopt the idea of Fernald's inversion method (Fernald et al., 1972) by assuming that a proportionality exists between the backscattering coefficient and the extinction coefficient of aerosols and atmospheric molecules:

$$S_a = \frac{\alpha_a(z)}{\beta_a(z)}, \tag{2}$$

$$S_m = \frac{\alpha_m(z)}{\beta_m(z)} = \frac{8\pi}{3}, \tag{3}$$

where $\alpha(z)$ is the extinction coefficient, $\beta(z)$ is the backscattering coefficient, and the subscripts a and m represent aerosol particles and atmospheric molecules, respectively. The ratio between the extinction coefficient of aerosols and its backscattering coefficient is also called the lidar ratio, which generally takes a value between 20 and 70 sr (Klett, 1981). The ratio of the extinction coefficient of an atmospheric molecule to its backscattering coefficient is calculated by derivation of the Rayleigh scattering formula (Thalman et al., 2014). This is the main theoretical basis for the simulation of the Mie–Rayleigh scattering lidar system.

2.2 Earth's Atmospheric Mode

The performance of a lidar system is closely related to the atmospheric environment in which it is located, so modeling of the atmospheric environment is critical to the simulation of a

Mie–Rayleigh scattering lidar system. To describe the atmospheric environment as reasonably as possible, we adopt the 1976 U.S. Standard Atmosphere model (U.S. Standard Atmosphere, 1976).

The 1976 U.S. Standard Atmosphere model takes the geographic sea level at latitude 45°32′33″ as a reference and sets the sea level temperature T_o = 288.15 K, atmospheric density ρ_0 = 1.225 kg/m^3, standard air pressure at sea level P_0 = 101325 Pa, and the average molecular weight of air M_0 = 28.9644 g/mol. The U.S. Standard Atmosphere model divides the effects on atmospheric backscattering and extinction into two parts: atmospheric molecules and aerosols.

The backscattering coefficient and extinction coefficient of atmospheric molecules can be expressed as follows (Fernald, 1984):

$$\beta_m(\lambda, z) = 1.54 \times 10^{-3} \exp\left(-\frac{z}{7}\right)\left(\frac{532}{\lambda}\right)^4, \tag{4}$$

$$\alpha_m(\lambda, z) = S_m(\lambda) \times \beta_m(\lambda, z), \tag{5}$$

The backscattering coefficient and extinction coefficient of aerosol particles can be expressed as follows (Fernald, 1984):

$$\beta_a(\lambda, z) = \left\{2.47 \times 10^{-3} \exp\left(-\frac{z}{2}\right) + 5.13 \times 10^{-6} \exp\left[-\frac{(z-20)^2}{36}\right]\right\}\left(\frac{532}{\lambda}\right), \tag{6}$$

$$\alpha_a(\lambda, z) = S_a(\lambda) \times \beta_a(\lambda, z). \tag{7}$$

In the equations above, z is the height in kilometers from the lidar, and λ is the wavelength of incident light in nanometers.

The total atmospheric extinction coefficient can be expressed as follows:

$$\alpha(z, \lambda) = \alpha_m(z, \lambda) + \alpha_a(z, \lambda). \tag{8}$$

Figure 1 shows the vertical distribution profile of atmospheric molecules and aerosol particles and the total extinction coefficient corresponding to the laser wavelength of 532 nm in the altitude range of 0–40 km.

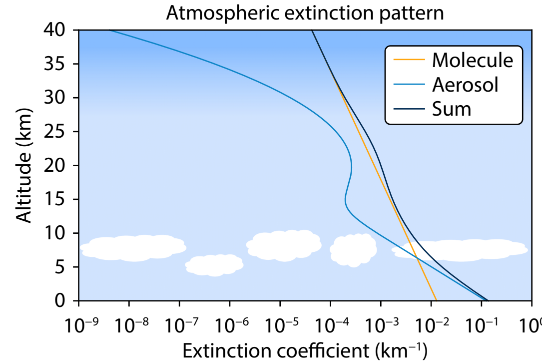

Figure 1. Atmospheric extinction mode in the U.S. Standard Atmosphere model.

2.3 Martian Atmospheric Mode

Fewer studies of the Martian atmosphere have been conducted, and no recognized atmospheric model exists like the U.S. Standard Atmosphere model on Earth. We choose the Mars Climate Database to characterize the Martian atmosphere.

The Mars Climate Database is a database of atmospheric statistics compiled from state-of-the-art Global Climate Model simulations of the Martian atmosphere (Montmessin, 2004; Madeleine et al., 2011). The database contains several statistics on simulated data stored on a 5.625° × 3.75° longitude–latitude grid from the surface up to an approximate altitude of 300 km. Fields are averaged and stored 12 times a day for 12 Martian “months” to give a comprehensive representation of the annual and diurnal cycles. Each month covers 30° in solar longitude (L_s) and is typically 50–70 Earth days long. In other words, at every grid point, the database contains 12 “typical” days, one for each month. In addition, information on the variability of the data within one month and the day-to-day oscillations is stored in the database.

For the selection of specific geographical locations on Mars, we select the corresponding data on the corresponding latitude and longitude grid with reference to the landing location of Tianwen-1. Pictures are available that depict the specific landing location and landing conditions of Tianwen-1, as shown in Figures 2a and 2b. From the large amount of data, we mainly use the atmospheric density. Figure 2c shows the distribution of the atmospheric molecular density of the atmosphere on Mars at a vertical distance of 0–40 km.

3. Simulation of the Mie–Rayleigh Scattering Lidar System

3.1 Parameter Design of the Ground-based Lidar System

According to the existing lidar systems at home and abroad, combined with the existing types of lasers, on the basis of considering the working environment and working requirements of the system, the parameters of the Mie–Rayleigh scattering lidar

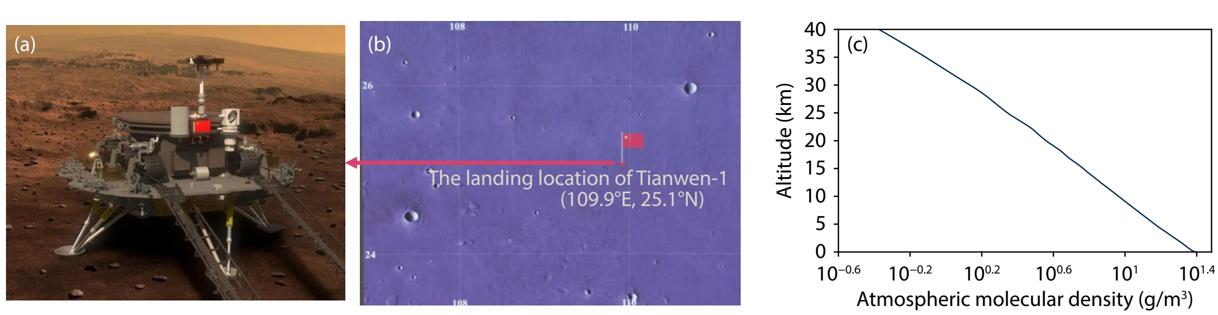

Figure 2. (a) The landing conditions of Tianwen-1. (b) The landing location of Tianwen-1. (c) Density profile of the atmospheric molecules on Mars.

system are temporarily determined for simulation and calculation. The specific parameters of the system used for simulation are listed in Table 1.

3.2 System Simulation in Earth's Atmospheric Mode

By substituting the relevant data on the Earth's atmosphere and the technical parameters of the lidar system into the lidar equation, the single-pulse backscattering photon counts of Rayleigh scattering lidar within the vertical distance of 0–40 km in the Earth's atmosphere mode can be simulated, as shown in Figure 3.

For the incident light wavelength λ = 532 nm, the daytime sky background light irradiance is generally 0.142 W/nm/m^2/sr. We choose a cumulative time of 1 min and further simulate the signal-to-noise ratio of the backscattering Rayleigh signal at the corresponding height, as shown in Figure 3.

3.3 Theoretical Demonstration of Simulation Results in Earth's Atmospheric Mode

To demonstrate the reliability of the simulation design, we compare the simulation results of the backscattering Rayleigh signal with the actual data collected by the Rayleigh lidar system at the University of Science and Technology of China.

As shown in Figure 4, the simulated Rayleigh backscattering photon number curve is compared with the measured Rayleigh backscattering photon number curve. In terms of the overall trend, the simulation results are consistent with the measured data. However, it is also clear that the measured data will be orders of magnitude smaller than the simulation results, which may be because the efficiency of the lidar system cannot reach the theoretical value in actual detection. In the actual detection process, in the altitude range below 15 km, the Mie backscattering signal is extremely strong, which will greatly interfere with the Rayleigh scattering signal. The Rayleigh backscattering signal in this region is truncated by an optical chopper. The detailed design of this Rayleigh lidar can be found in Ma J et al. (2019).

The calculation of the signal-to-noise ratio in Section 3.2 is considered in an ideal situation, in which we consider that the interference of the Mie scattering signal to the Rayleigh backscattering signal can be completely filtered. However, in practice, this assumption is unlikely to be realized because the Mie scattering signal intensity is 2–3 orders of magnitude larger than that of the Rayleigh. Although narrow-band filters can be used to filter out most of the Mie scattering signal in the receiving part of the Rayleigh scattering lidar system, the remaining fraction of the Mie scattering signal in the low-altitude range is still a large noise disturbance relative to the Rayleigh backscattering signal. At present, the commonly used filter device can filter out approximately 90% of the Mie backscattering signal. To describe the working performance of the

Table 1. Technical parameters of the Mie–Rayleigh scattering lidar system.

	Parameter	Value
Laser	Laser wavelength	532 nm
	Laser energy	300 mJ
	Repetition rate	20 Hz
	Pulse width	20 ns
	Optical transmittance of the transmitting unit	70%
Telescope	Diameter	0.4 m
	View angle of receiving field	0.5 mrad
	Optical transmittance of receiving unit	70%
Detector	Narrow-band filter bandwidth	1.9 nm
	Quantum efficiency	25%
	Optical efficiency	10%
	Vertical resolution	15 m
	Dark count	500 count/s

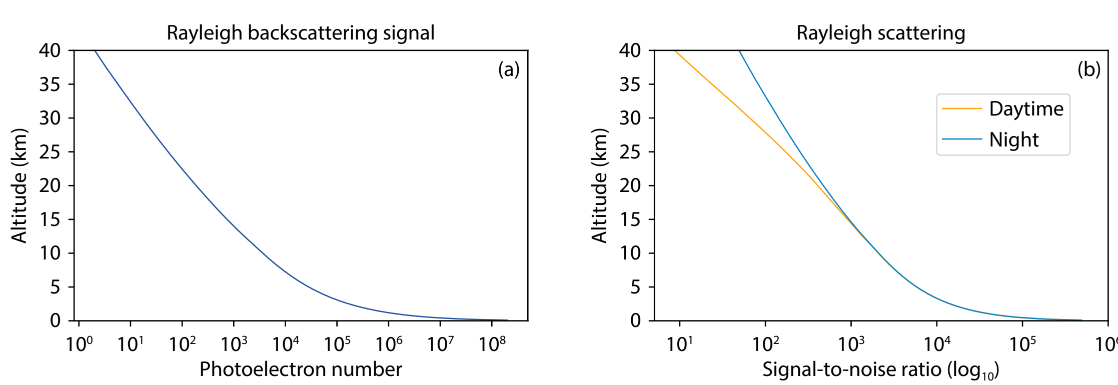

Figure 3. (a) Backscattering signal simulation results of Rayleigh scattering lidar. (b) Simulation results of the signal-to-noise ratio.

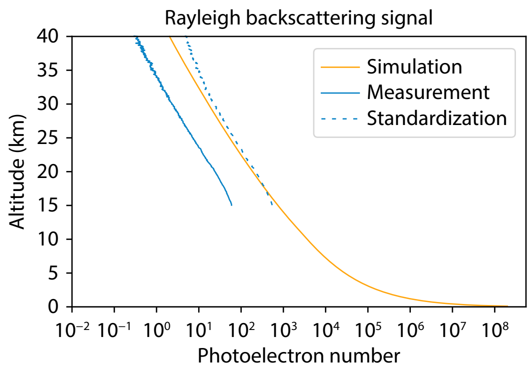

Figure 4. Comparison between simulation results and measured results of the Rayleigh backscattering signal.

lidar system in the atmospheric environment more realistically and reasonably, we take into account the interference of the Mie scattering signal and simulate the signal-to-noise ratio of the system again. Figure 5 shows the corresponding signal-to-noise ratio simulation results in the Earth's atmospheric mode under daytime conditions when the cumulative time is 10, 20, and 30 min.

The cumulative time is determined to be 20 min, that is, the cumulative number of pulses is 24,000. For a more intuitive comparative analysis, we plot the signal-to-noise ratio simulation curve with the Mie scattering signal as noise and the Rayleigh scattering signal as the useful signal, and the signal-to-noise ratio simulation curve with the Rayleigh scattering signal as noise and the Mie scattering signal as the useful signal in the same coordinate image, as shown in Figure 5.

In Figure 5, when the Mie backscattering signal is used as a useful signal in the vertical height range below 30 km, the signal-to-noise ratio is obviously better, so it is more reasonable and suitable to use the Mie backscattering signal to invert the wind field or other atmospheric characteristics in this height range. In a specific altitude range above 30 km, the signal-to-noise ratio is better when the Rayleigh backscattering signal is used as a useful signal. In the Earth's atmospheric mode, this conclusion obtained from the simulation results is also highly consistent with the actual application (Rees et al., 1996; Zhang JY et al., 2008). This result fully demonstrates the feasibility and rationality of the simulation.

3.4 Revised Model of the Martian Atmosphere

Approximately 95% of the gas composition in the Martian atmosphere is CO_2 (Niles et al., 2010), so calculation of the Rayleigh scattering differential backscatter cross-section and backscatter coefficient is directly based on the molecular correlation characteristics of CO_2 gas when simulating the operation of the lidar system on Mars. It can be deduced from the relevant theoretical knowledge that when the wavelength of the incident light is in nanometers, the differential backscattering cross-section value of CO_2 molecules is approximately 1.17×10^{-30} m^2/sr (Ityaksov et al., 2008). In addition, the backscattering coefficient of atmospheric molecules on Mars within the vertical distance range of 0–40 km in a clean atmospheric environment and with a large distribution of aerosols is obtained by simulation, as shown in Figure 6. It is obvious from Figure 6 that the content and distribution of Martian atmospheric molecules are relatively stable, although the content of aerosols is obviously different.

For the characteristics of aerosols in the Martian atmosphere, relevant detection data are currently lacking. Considering that the content and distribution of aerosols on Mars are relatively variable, to improve the universality and authenticity of the simulation, a clean atmosphere and the occurrence of global dust storms on Mars are selected, respectively. In the case of the clean atmosphere, the content and distribution of aerosols in the Martian atmosphere are replaced by aerosol-related data in the U.S. Standard Atmosphere model. The content and distribution status of aerosols in the case of global dust storms on Mars are replaced by aerosol-related data over the desert during the occurrence of dust storms on Earth, which can be used to reasonably describe the characteristics of aerosols in the Martian atmosphere.

From June 14 to June 19, 2020, a dust storm of exceptional magnitude occurred over the Sahara Desert, which had the largest aerosol optical thickness since June 2002 (Asutosh et al., 2022). The CALIOP (Cloud-Aerosol Lidar with Orthogonal Polarization) instrument aboard the CALIPSO (Cloud-Aerosol Lidar and Infrared Pathfinder Satellite Observation; Winker et al., 2003) satellite detected the relevant data.

The CALIPSO satellite data are divided into three levels (Level 0, Level 1, and Level 2) that contain different types of data (Vaughan et al., 2004). The aerosol profile data in Level 2 of the corresponding CALIPSO satellite over the Sahara Desert for the time period from

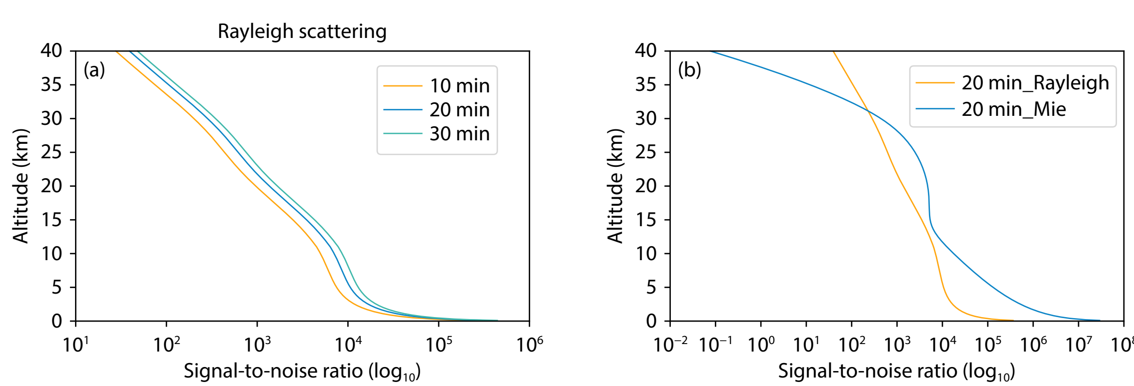

Figure 5. (a) Simulation results of the signal-to-noise ratio of the Rayleigh backscattering signal under different accumulation times. (b) Comparison of signal-to-noise ratio simulation curves under different signal conditions.

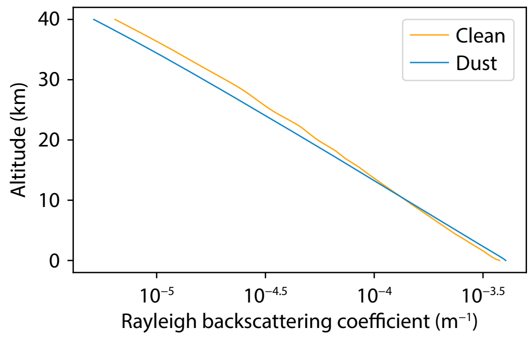

Figure 6. Molecular backscatter coefficient of the Martian atmosphere under different atmospheric conditions.

June 14 to June 19, 2020, were obtained from the NASA official website. A total of 33 data files corresponded to the relevant data detected by the satellite over the Sahara Desert on 33 passes during that time period. One extinction coefficient profile had 399 data points in the vertical distance of 0–20 km, but the distribution of data in the vertical direction was not uniform. We found, after reading the data, that the aerosol extinction coefficient data were concentrated in only a small altitude range and that no valid aerosol data were available in most of the vertical space. Note that the vertical coordinates in the figures indicate only points at different altitudes and do not have actual physical units, and the horizontal coordinates indicate only different positions on the satellite trajectory and do not have actual physical meaning.

Obviously, it is not reasonable to use the aerosol extinction coefficient profiles obtained from the inversion of CALIPSO remote sensing data directly, without any processing. Figure 7 shows a flowchart for processing the CALIPSO satellite remote sensing data that meets the qualification conditions and can be used directly as a substitute for aerosol characterization data in the Martian atmosphere in the case of a global dust storm. Considering the high aerosol content in the Martian atmosphere, first, to compare the 33 groups of acquired data, we select the specific data corresponding to a section of the flight track with relatively large aerosol extinction coefficients. Second, we perform averaging in the dimension of the position to minimize the interference of some extreme value points. We then select the continuous effective value part of the extinction coefficient profile. This part of the effective value is then interpolated to be considered the aerosol extinction coefficient data for the range of vertical distances from 0 to 40 km over Mars, which can be used to substitute for modeling the lacking aerosol portion of the Martian atmospheric mode.

4. Analysis of the Simulation Results

After establishing a complete model of the Martian atmosphere, the operating performance of the Rayleigh scattering lidar in the Martian atmospheric environment can be simulated according to the simulation steps in the Earth's atmospheric mode. Considering that the content, distribution, and other characteristics of aerosols in the Martian atmosphere change drastically with time and climate, two conditions, a low and a high aerosol content, representing a relatively clean atmosphere and a global dust storm, are selected for simulation from the corresponding data on 12 Martian months. The parameters of the lidar system, accumulation time, and other parameters are chosen to be consistent with the simulation in the Earth's atmospheric mode.

4.1 Situations with a Low Aerosol Content

The aerosol content of the clean Martian atmosphere is replaced by the correlation of aerosols in the U.S. Standard Atmosphere model. The specific simulated Rayleigh scattering lidar backscattering photon counts and signal-to-noise ratios for the system at night are shown in Figures 8a and 8b.

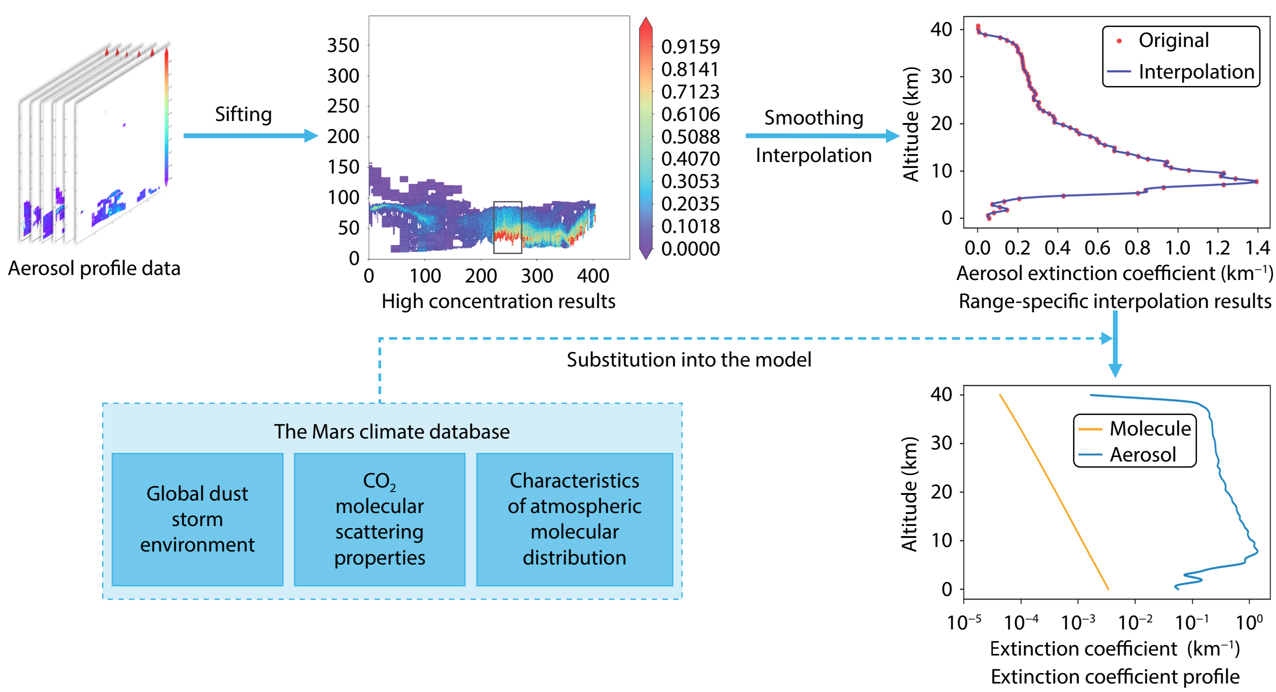

Figure 7. Schematic diagram of the partial data processing flow for aerosols during dust storms.

4.2 Situations with a High Aerosol Content

In the case of a high aerosol content in the Martian atmosphere, the aerosol-related characterization data are replaced by the processed data over the Sahara Desert described above. The simulated Rayleigh scattering lidar return photon counts and the signal-to-noise ratio of the system at night are shown in Figures 8c and 8d.

After verifying the correctness of the simulation results in the Earth's atmospheric mode, we can also adopt the same idea in the Martian atmospheric mode to determine the altitude range in which it is more suitable and appropriate to use the Mie backscattering signals and Rayleigh backscattering signals, respectively, to invert the wind field of the lidar system operating in the Martian atmospheric environment. The following two scenarios are still typical of the Mars atmospheric mode during global dust storms, that is, the clean atmospheric and aerosol-heavy scenarios.

4.3 Situations with a Low Aerosol Content

In the relatively clean atmospheric conditions on Mars, we first simulate the Mie backscattering signals received by the lidar system separately. We then carry out the corresponding signal-to-noise ratio simulations by treating the Rayleigh backscattering signals as useful signals and the Mie scattering signals as noise and by treating the Mie backscattering signals as useful signals and the Rayleigh scattering signals as noise.

Figures 9a and 9b show the simulation results of the signal-to-noise ratio with the Rayleigh backscattering signal as the useful signal and with the Mie backscattering signal as the useful signal, respectively, within different accumulation times. With a fixed accumulation time of 20 min, the above-mentioned two signal-to-noise ratio simulation results are plotted in the same coordinate image, as shown in Figure 9c.

From Figure 9, in the altitude range of 0–33.5 km, the signal-to-noise ratio of the Mie backscattering signal as the useful signal can clearly be seen as advantageous. In the altitude range of more than 33.5 km, the signal-to-noise ratio of the Rayleigh backscattering signal as the useful signal can be seen as advantageous. Therefore, in the case of a relatively clean atmosphere in the Martian atmospheric environment, when the lidar system is used to detect atmospheric characteristics such as wind fields, the Mie backscattering signal is selected within the vertical distance and height range of 0–33.5 km for inversion of the corresponding characteristics, and the information on the Rayleigh backscattering signal is selected within the height range of more than 33.5 km. This detection program is more reasonable, and the detection effect will be better. Thus, we can realize the continuous detection of Martian atmospheric properties and the inversion of temperature and wind fields from the surface to the middle and upper layers in the cleaner atmospheric environment of Mars.

4.4 Situations with a High Aerosol Content

In the case of a large aerosol content, the corresponding signal-to-noise ratio simulation calculations are carried out with the Mie scattering signal as the useful signal and with the Rayleigh scattering signal as the useful signal, respectively, according to similar analytical ideas. When the accumulation time is fixed at 20 min,

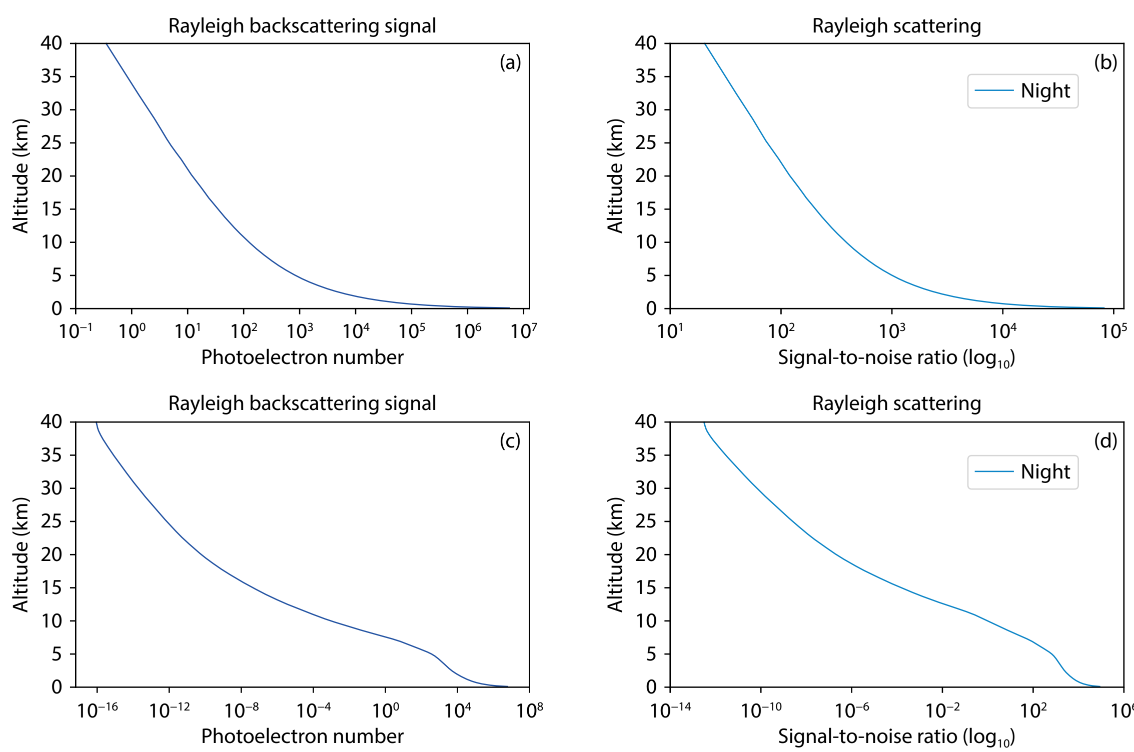

Figure 8. Simulation results. (a) Rayleigh backscattering signal in the Martian atmospheric mode (clean atmosphere). (b) Signal-to-noise ratio in the Martian atmospheric mode (clean atmosphere). (c) Rayleigh backscattering signal in the Martian atmospheric mode (a global dust storm). (d) Signal-to-noise ratio in the Martian atmospheric mode (a global dust storm).

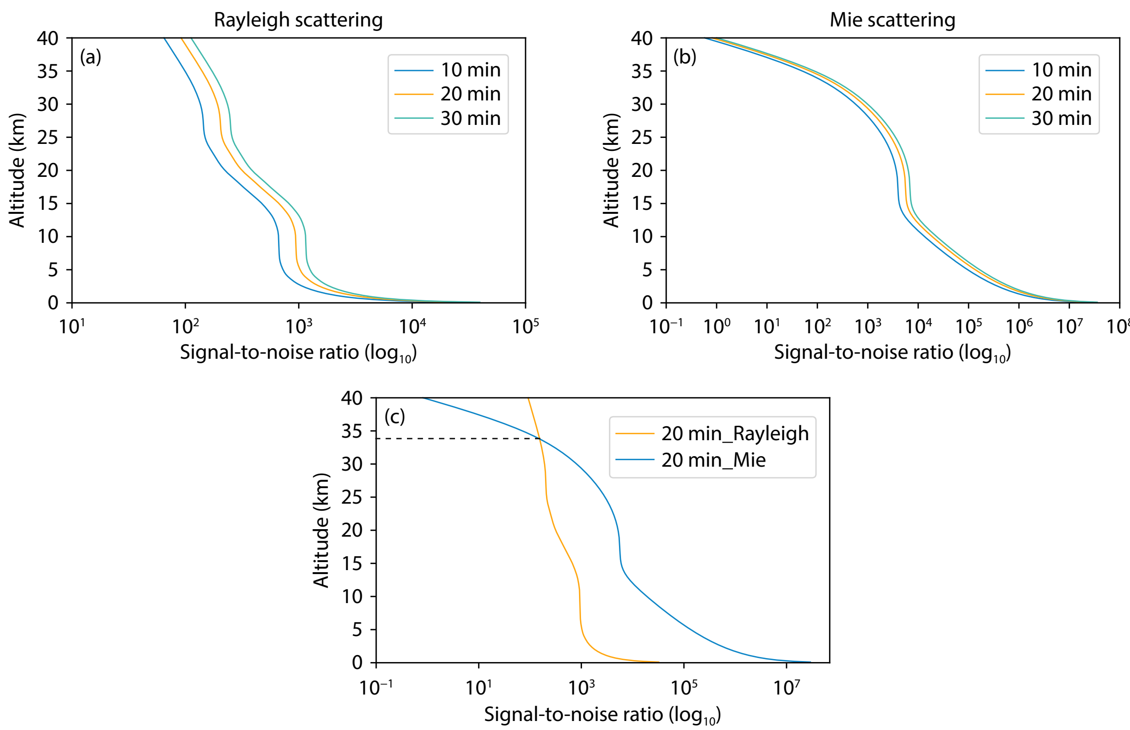

Figure 9. Simulation results of the signal-to-noise ratio for the clean atmosphere case of the Martian atmospheric mode. (a) Rayleigh backscattering signal as the useful signal. (b) Mie backscattering signal as the useful signal. (c) Comparison of different types of signal-to-noise ratio simulations.

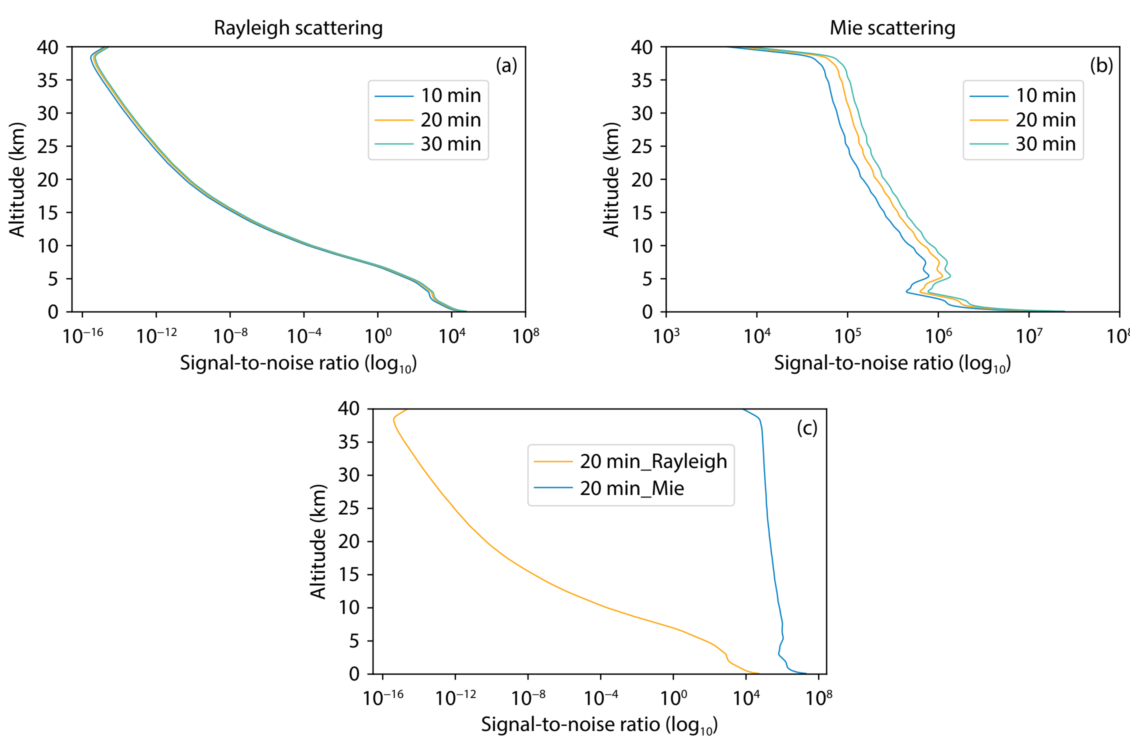

Figure 10. Simulation results of the signal-to-noise ratio in the case of a global dust storm in the Martian atmospheric mode. (a) Rayleigh backscattering signal as the useful signal. (b) Mie backscattering signal as the useful signal. (c) Comparison of the different types of signal-to-noise ratio simulations.

the signal-to-noise ratio curves of the two are neutralized to the same coordinate image, which is convenient for comparison and analysis.

Figure 10 shows the simulation results of the signal-to-noise ratio with the Rayleigh backscattering signal as the useful signal and the simulation results of the signal-to-noise ratio with the Mie scattering signal as the useful signal within different accumulation times. The fixed accumulation time is 20 min, and the comparison result of the two is shown in Figure 10c.

The atmosphere on Mars during global dust storms is extremely harsh, with an extremely wide range of aerosols and extremely high aerosol concentrations. At this time, the intensity of the signal returned by the Mie scattering interaction between the laser and the aerosol particles will be much greater than the intensity of the Rayleigh backscattering signal. The three images in Figures 10a–10c also clearly reflect this, so in this case, the Mie scattering signal in the range of 0–40 km is theoretically more suitable for the inversion of relevant atmospheric information. However, in practical applications, the effectiveness of the Mie backscattering signal in such extremely harsh conditions is also worth investigating.

To simulate an atmospheric environment in which the aerosol content on Mars is between the two extremes of a clean atmosphere and a global dust storm, the aerosol content and distribution data used in a clean atmosphere are “multiply” processed to replace them accordingly. According to the same simulation process, we simulate the working state of the Mie–Rayleigh scattering lidar system under various aerosol contents in the Martian atmospheric environment. The simulation results are analyzed theoretically according to the above-mentioned analytic process, and the specific analytic process will not be repeated here. The theoretical boundary height value of the lidar system is obtained under different “multiple” processing steps. As shown in Figure 11, the image of the theoretical demarcation height value of the preferred Mie scattering signal or the Rayleigh scattering signal of the lidar system changes with different processing multiples, that is, a change in the boundary height value corresponds to the different aerosol contents in the Martian atmosphere.

This curve describes the optimal detection altitude range for Mie scattering and Rayleigh scattering in the Martian atmosphere under different aerosol contents. These results will directly determine which channel signals are selected at different heights in the data processing section under different atmospheric conditions on Mars. Moreover, these results will help us select the bandwidth parameters of the filter and set the height at which the different detectors begin to collect data. In detail, the signal acquisition part of the Mie–Rayleigh scattering lidar is usually divided into two channels. Photon detectors are usually used to collect Rayleigh scattering signals, and photomultiplier tubes are used to collect Mie scattering signals. However, to prevent the influence of the backscattering signal reflected by low-altitude aerosols on the Rayleigh scattering signal and to avoid detector saturation, it is necessary to set the height at which the photon detector begins collecting data. The setting of this height value is directly related to the optimal detection altitude range of Mie scattering and Rayleigh scattering. These are just a few examples of the applications of these results to assist in the parameter design of Mie–Rayleigh scattering lidar. This curve no doubt provides a theoretical basis for the subsequent design of Mars atmospheric exploration using the Mie–Rayleigh scattering lidar system under different aerosol contents.

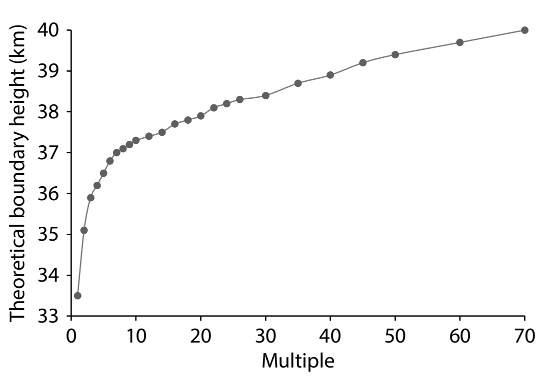

Figure 11. Change curve of the theoretical demarcation height value with different treatment multiples.

5. Conclusions

Mie–Rayleigh scattering lidar is an important technique to detect parameters from the surface to the middle and upper atmosphere, but Mie scattering and Rayleigh scattering have optimal detection intervals in atmospheric detection. To realize continuous detection, the interface position of the two needs to be optimized. On the basis of the existing theory, this study first models the Mie–Rayleigh scattering lidar system for Mars. In the Earth’s atmospheric mode, the working performance of the system is analyzed theoretically. The simulation results are compared with the measured data on Rayleigh lidar from the University of Science and Technology of China, and the conclusions obtained are highly consistent with practical applications. This result fully demonstrates the rationality of the simulation design scheme of our Mie–Rayleigh scattering lidar system and shows that simulation has great reference value for actual design. The source data on the Mars atmospheric model come from the Mars climate database, and some assumptions and data processing are carried out on this basis to improve the model. According to the theoretical simulation process and analytic method of the ground-based Mie–Rayleigh scattering lidar system, the working state of the Mie–Rayleigh scattering lidar system in the Martian atmospheric mode is simulated, and the simulation results are analyzed.

The theoretical conclusions obtained from the analysis are as follows:

(1) In a relatively clean Martian atmospheric environment, when the lidar system is used to detect atmospheric characteristics, the Mie backscattering signal is preferred in the altitude range of 0–33.5 km, and the Rayleigh backscattering signal is preferred in the altitude range above 33.5 km.

(2) During a global dust storm on Mars, the content of aerosol particles in the atmosphere is extremely high, the distribution range is extremely wide, and the signal intensity returned by the laser scattering interaction with the aerosol particles is much

greater than the intensity of the Rayleigh backscattering signal. Theoretically, in this case, the Mie scattering signal would be more suitable for the inversion of relevant atmospheric information. However, the feasibility of detecting the atmosphere by visible light in such extreme conditions is still a topic of debate.

The theoretical conclusions obtained by our analysis provide a reference for the subsequent practical design and development of lidar systems for the Martian atmospheric environment. At the same time, Mars is a typical terrestrial planet, and the work done in this project also provides a direction for thinking and a reasonable reference for the atmospheric exploration of other terrestrial planets in the future.

Acknowledgments

We acknowledge financial support from the B-type Strategic Priority Program of the Chinese Academy of Sciences (Grant No. XDB41030000), the National Natural Science Foundation of China (Grant Nos. 42125402, 42188101, 42304165, and 42374182), the Key-Area Research and Development Program of Guangdong Province (Grant No. 2020B0303020001), the Shanghai Municipal Science and Technology Major Project (Grant No. 2019SHZDZX01), and the Innovation Program for Quantum Science and Technology (Grant No. 2021ZD0300302), "Study on the interaction between low/mid-latitude atmosphere and ionosphere based on the Chinese Meridian Project."

Disclosures

The authors declare no conflicts of interest.

Data Availability

Data underlying the results presented in this paper are not publicly available at this time but may be obtained from the authors upon reasonable request.

References

Abedin, M. N., Bradley, A. T., Sharma, S. K., Misra, A. K., Lucey, P. G., McKay, C. P., Ismail, S., and Sandford, S. P. (2015). Mineralogy and astrobiology detection using laser remote sensing instrument. *Appl. Opt.*, *54*(25), 7598–7611. https://doi.org/10.1364/AO.54.007598

Asaka, K., Yanagisawa, T., and Hirano, Y. (2001). 1.5-µm eye-safe coherent lidar system for wind velocity measurement. In *Proceedings Volume 4153, Lidar Remote Sensing for Industry and Environment Monitoring* (pp. 321–328). Sendai, Japan: SPIE. https://doi.org/10.1117/12.417063

Asutosh, A., Vinoj, V., Murukesh, N., Ramisetty, R., and Mittal, N. (2022). Investigation of June 2020 giant Saharan dust storm using remote sensing observations and model reanalysis. *Sci. Rep.*, *12*, 6114. https://doi.org/10.1038/s41598-022-10017-1

Cremons, D. R., Abshire, J., Allan, G., Sun, X. D., Riris, H., Smith, M., Guzewich, S., Yu, A., and Hovis, F. (2018). Development of a Mars lidar (MARLI) for measuring wind and aerosol profiles from orbit. In *Proceedings Volume 10791, Lidar Technologies, Techniques, and Measurements for Atmospheric Remote Sensing XIV* (pp. 22–34). Berlin, Germany: SPIE. https://doi.org/10.1117/12.2325408

Dou, X. K., Han, Y. L., Sun, D. S., Xia, H. Y., Shu, Z. F., Zhao, R. C., Shangguan, M. J., and Guo, J. (2014). Mobile Rayleigh Doppler lidar for wind and temperature measurements in the stratosphere and lower mesosphere. *Opt. Express*, *22*(S5), A1203–A1221. https://doi.org/10.1364/OE.22.0A1203

Fernald, F. G., Herman, B. M., and Reagan, J. A. (1972). Determination of aerosol height distributions by Lidar. *J. Appl. Meteor.*, *11*(3), 482–489. https://doi.org/10.1175/1520-0450(1972)011<0482:DOAHDB>2.0.CO;2

Fernald, F. G. (1984). Analysis of atmospheric lidar observations: Some comments. *Appl. Opt.*, *23*(5), 652–653. https://doi.org/10.1364/AO.23.000652

Frehlich, R., Hannon, S. M., and Henderson, S. W. (1994). Performance of a 2-µm coherent Doppler lidar for wind measurements. *J. Atmos. Oceanic Technol.*, *11*(6), 1517–1528. https://doi.org/10.1175/1520-0426(1994)011<1517:POACDL>2.0.CO;2

Hong, G. L., Zhou, Y. B., Liu, H., Kong, W., and Shu, R. (2018). Feasibility study of Mars Rover's laser induced breakdown spectroscopy based Mie-Lidar design. *Spectroscopy and Spectral Analysis*, *38*(2), 600–605 https://doi.org/10.3964/j.issn.1000-0593(2018)02-0600-06

Ityaksov, D., Linnartz, H., and Ubachs, W. (2008). Deep-UV absorption and Rayleigh scattering of carbon dioxide. *Chem. Phys. Lett.*, *462*(1-3), 31–34. https://doi.org/10.1016/j.cplett.2008.07.049

Klett, J. D. (1981). Stable analytical inversion solution for processing lidar returns. *Appl. Opt.*, *20*(2), 211–220. https://doi.org/10.1364/AO.20.000211

Komguem, L., Whiteway, J. A., Dickinson, C., Daly, M., and Lemmon, M. T. (2013). Phoenix LIDAR measurements of Mars atmospheric dust. *Icarus*, *223*(2), 649–653. https://doi.org/10.1016/j.icarus.2013.01.020

Li, Y. D., Wang, C., Xue, X. H., Wang, Y., Shang, X., Jia, M. J., and Chen, T. D. (2022). Study on the parameters of ice clouds based on 1.5 µm micropulse polarization lidar. *Remote Sens.*, *14*(20), 5162. https://doi.org/10.3390/rs14205162

Li, Z. G., Sun, Z. Z., Zhao, Z. L., Zhu, X. P., and Zhu, J. S. (2016). Wind retrieval of airborne fiber Doppler wind lidar and experimental verification. *J. Appl. Opt. (in Chinese)*, *37*(5), 618–622. https://doi.org/10.5768/JAO201637.0507001

Ma, J., Shangguan, M. J., Xia, H. Y., Fang, X., Xue, X. H., and Dou, X. K. (2019). Rayleigh and sodium lidar system incorporating time-division and wavelength-division multiplexing. *Opt. Commun.*, *448*, 116–123. https://doi.org/10.1016/j.optcom.2019.05.010

Madeleine, J. B., Forget, F., Millour, E., Montabone, L., and Wolff, M. J. (2011). Revisiting the radiative impact of dust on Mars using the LMD Global Climate Model. *J. Geophys. Res.: Planets*, *116*(E11), E11010. https://doi.org/10.1029/2011JE003855

Montmessin, F., Forget, F., Rannou, P., Cabane, M., and Haberle, R. M. (2004). Origin and role of water ice clouds in the Martian water cycle as inferred from a general circulation model. *J. Geophys. Res.: Planets*, *109*(E10), E10004. https://doi.org/10.1029/2004JE002284

Niles, P. B., Boynton, W. V., Hoffman, J. H., Ming, D. W., and Hamara, D. (2010). Stable isotope measurements of Martian atmospheric CO_2 at the Phoenix landing site. *Science*, *329*(5997), 1334–1337. https://doi.org/10.1126/science.1192863

Paffrath, U., Lemmerz, C., Reitebuch, O., Witschas, B., Nikolaus, I., and Freudenthaler, V. (2009). The airborne demonstrator for the direct-detection Doppler wind lidar ALADIN on ADM-Aeolus. Part II: Simulations and Rayleigh receiver radiometric performance. *J. Atmos. Oceanic Technol.*, *26*(12), 2516–2530. https://doi.org/10.1175/2009JTECHA1314.1

Rees, D., Vyssogorets, M., Meredith, N. P., Griffin, E., and Chaxell, Y. (1996). The Doppler wind and temperature system of the ALOMAR lidar facility: Overview and initial results. *J. Atmos. Terr. Phys.*, *58*(16), 1827–1842. https://doi.org/10.1016/0021-9169(95)00174-3

Reitebuch, O., Lemmerz, C., Nagel, E., Paffrath, U., Durand, Y., Endemann, M., Fabre, F., and Chaloupy, M. (2009). The airborne demonstrator for the direct-detection Doppler wind lidar ALADIN on ADM-Aeolus. Part I: Instrument design and comparison to satellite instrument. *J. Atmos. Oceanic Technol.*, *26*(12), 2501–2515. https://doi.org/10.1175/2009JTECHA1309.1

Shen, F. H., Wang, Z., Xia, Y. Q., Wang, B. X., Zhuang, P., and Qiu, C. Q. (2021). Quad-Fabry-Perot etalon based Rayleigh Doppler lidar for 0.2–60 km altitude wind, temperature and aerosol accurate measurement. *Optik*, *236*, 166668. https://doi.org/10.1016/j.ijleo.2021.166668

Sun, X. L., Abshire, J. B., Beck, J. D., Mitra, P., Reiff, K., and Yang, G. N. (2017). HgCdTe avalanche photodiode detectors for airborne and spaceborne lidar at infrared wavelengths. *Opt. Express*, *25*(14), 16589–16602. https://doi.org/10.1364/OE.25.016589

Thalman, R., Zarzana, K. J., Tolbert, M. A., and Volkamer, R. (2014). Rayleigh scattering cross-section measurements of nitrogen, argon, oxygen and air. *J. Quant. Spectrosc. Radiat. Transfer*, *147*, 171–177. https://doi.org/10.1016/j.jqsrt.2014.05.030

U.S. Standard Atmosphere, 1976 (No. NOAA-S/T-76-1562), 1976.

Vaughan, M. A., Young, S. A., Winker, D. M., Powell, K. A., Omar, A. H., Liu, Z. Y., Hu, Y. X., and Hostetler, C. A. (2004). Fully automated analysis of space-based lidar data: An overview of the CALIPSO retrieval algorithms and data products. In *Proceedings Volume 5575, Laser Radar Techniques for Atmospheric Sensing* (pp. 16–30). Maspalomas, Canary Islands, Spain: SPIE. https://doi.org/10.1117/12.572024

Whiteway, J., Daly, M., Carswell, A., Duck, T., Dickinson, C., Komguem, L., and Cook, C. (2008). Lidar on the Phoenix mission to Mars. *J. Geophys. Res.: Planets*, *113*(E3), E00A08. https://doi.org/10.1029/2007JE003002

Winker, D. M., Pelon, J. R., and McCormick, M. P. (2003). The CALIPSO mission: Spaceborne lidar for observation of aerosols and clouds. In *Proceedings Volume 4893, Lidar Remote Sensing for Industry and Environment Monitoring III* (pp. 1–11). Hangzhou, China: SPIE. https://doi.org/10.1117/12.466539

Yakovlev, S. V., Sadovnikov, S. A., and Romanovskii, O. A. (2022). Mobile airborne lidar for remote methane monitoring: Design, simulation of atmospheric measurements and first flight tests. *Remote Sens.*, *14*(24), 6355. https://doi.org/10.3390/rs14246355

Zhang, J. Y., Gong, W., Zhu, Z. M., Li, J., Li, P. X., Zhang, L. P., Song, S. L., Ma, Y. Y., Mao, F. Y., … Hu, Z. L. (2008). Development and new application of Raman/Mie lidar: Severe weather research and Earth observation atmospheric correction. In *Proceedings Volume 7003, Optical Sensors 2008* (pp. 617–622). Strasbourg, France: SPIE. https://doi.org/10.1117/12.781669